PNAS RESEARCH ARTICLE | NEUROSCIENCE OPEN ACCESS

Comprehensive evaluation of human-derived anti-poly-GA antibodies in cellular and animal models of *C9orf72* disease

Melanie Jambeau[a,b,c,1], Kevin D. Meyer[d,e,1], Marian Hruska-Plochan[c,1], Ricardos Tabet[a,b], Chao-Zong Lee[a,b], Ananya Ray-Soni[a,b], Corey Aguilar[a,b], Kitty Savage[a,b], Nibha Mishra[a,b], Nicole Cavegn[d], Petra Borter[d], Chun-Chia Lin[a], Karen R. Jansen-West[f], Jie Jiang[g], Fernande Freyermuth[a,b], Nan Li[a,b], Pierre De Rossi[c], Manuela Pérez-Berlanga[c], Xin Jiang[a,b], Lilian M. Daughrity[f], João Pereira[a,b], Sarav Narayanan[h], Yuanzheng Gu[h], Shekhar Dhokai[h], Isin Dalkilic-Liddle[h], Zuzanna Maniecka[c], Julien Weber[c], Michael Workman[a], Melissa McAlonis-Downes[g], Eugene Berezovski[a,b], Yong-Jie Zhang[f], James Berry[a], Brian J. Wainger[a,b], Mark W. Kankel[h], Mia Rushe[h], Christoph Hock[d,e], Roger M. Nitsch[d,e], Don W. Cleveland[g,2], Leonard Petrucelli[f], Tania F. Gendron[f], Fabio Montrasio[d], Jan Grimm[d,2], Magdalini Polymenidou[c,2], and Clotilde Lagier-Tourenne[a,b,2]

Contributed by Don W. Cleveland; received January 10, 2022; accepted September 27, 2022; reviewed by Kenneth H. Fischbeck and Harry T. Orr

Hexanucleotide G_4C_2 repeat expansions in the *C9orf72* gene are the most common genetic cause of amyotrophic lateral sclerosis and frontotemporal dementia. Dipeptide repeat proteins (DPRs) generated by translation of repeat-containing RNAs show toxic effects in vivo as well as in vitro and are key targets for therapeutic intervention. We generated human antibodies that bind DPRs with high affinity and specificity. Anti-GA antibodies engaged extra- and intra-cellular poly-GA and reduced aggregate formation in a poly-GA overexpressing human cell line. However, antibody treatment in human neuronal cultures synthesizing exogenous poly-GA resulted in the formation of large extracellular immune complexes and did not affect accumulation of intracellular poly-GA aggregates. Treatment with antibodies was also shown to directly alter the morphological and biochemical properties of poly-GA and to shift poly-GA/antibody complexes to more rapidly sedimenting ones. These alterations were not observed with poly-GP and have important implications for accurate measurement of poly-GA levels including the need to evaluate all centrifugation fractions and disrupt the interaction between treatment antibodies and poly-GA by denaturation. Targeting poly-GA and poly-GP in two mouse models expressing G_4C_2 repeats by systemic antibody delivery for up to 16 mo was well-tolerated and led to measurable brain penetration of antibodies. Long-term treatment with anti-GA antibodies produced improvement in an open-field movement test in aged *C9orf72*^{450} mice. However, chronic administration of anti-GA antibodies in AAV-$(G_4C_2)_{149}$ mice was associated with increased levels of poly-GA detected by immunoassay and did not significantly reduce poly-GA aggregates or alleviate disease progression in this model.

C9orf72 | amyotrophic lateral sclerosis | frontotemporal dementia | immunotherapy | dipeptide repeat proteins

Hexanucleotide repeat expansions (G_4C_2) in the *C9orf72* gene are the most frequent genetic cause of amyotrophic lateral sclerosis (ALS) and frontotemporal dementia (FTD) (1, 2). Proposed disease mechanisms include *C9orf72* haploinsufficiency, repeat-RNA toxicity, and protein toxicity. Though the relative contribution of each mechanism is not fully understood (3), there is mounting evidence that accumulation of dipeptide repeat proteins (DPRs), generated by repeat-associated non-ATG (RAN) translation across the *C9orf72* expansion plays a crucial role in neurodegeneration (4–9). DPRs are translated from both sense (poly-GA, poly-GR, and poly-GP) and antisense (poly-PR, poly-PA, and poly-GP) repeat-containing RNAs and represent the major component of p62-positive, TDP-43-negative aggregates in the central nervous system of *C9orf72* ALS/FTD patients (10–12). Moreover, several in vivo and in vitro studies support direct toxic effects of arginine-rich DPR proteins poly-PR and poly-GR (13–17), as well as the aggregation-prone and most abundant DPR product, poly-GA (18–20). A recent study directly comparing congenic mice expressing either poly-GA or poly-PR indicates that poly-GA is considerably more toxic, leading to TDP-43 abnormalities and neuronal loss (21), highlighting its suitability as a therapeutic target.

Passive immunotherapy using humanized or fully human antibodies targeting aberrantly produced or misfolded proteins has been investigated in several preclinical and clinical settings for the treatment of neurodegenerative disorders (22, 23). The most advanced programs have targeted extracellular amyloid-β plaques in mouse models and patients with Alzheimer's disease (24, 25). Targeting intracellular misfolded proteins, including tau and α-synuclein, has also shown beneficial effects on pathology and behavioral abnormalities in multiple mouse models of Alzheimer's (26, 27) or Parkinson's

Significance

Immunotherapy has been proposed for neurodegenerative disorders including Alzheimer's disease. Recent reports using antibodies against poly-GA or active immunization suggested similar immunotherapy in ALS/FTD caused by repeat expansion in the *C9orf72* gene. Here, we systematically characterized human antibodies against multiple DPR species and tested the biological effects of antibodies targeting poly-GA in different cellular and mouse models. Target engagement was shown in three independent cellular models. Anti-GA antibodies reduced the number of intracellular poly-GA aggregates in human T98G cells but not in cultured human neurons. Chronic anti-GA treatment in BAC *C9orf72*^{450} mice did not impact poly-GA levels and modestly improved one behavioral phenotype, whereas poly-GA levels detected by immunoassays were increased and disease progression was unaltered in AAV-$(G_4C_2)_{149}$ mice.

Copyright © 2022 the Author(s). Published by PNAS. This open access article is distributed under Creative Commons Attribution-NonCommercial-NoDerivatives License 4.0 (CC BY-NC-ND).

[1]M.J., K.D.M., and M.H.-P. contributed equally to this work.

[2]To whom correspondence may be addressed. Email: dcleveland@health.ucsd.edu, jan.grimm@neurimmune.com, magdalini.polymenidou@uzh.ch, or clagier-tourenne@mgh.harvard.edu.

This article contains supporting information online at https://www.pnas.org/lookup/suppl/doi:10.1073/pnas.2123487119/-/DCSupplemental.

Published December 1, 2022.

diseases (28). Recently, human-derived antibodies targeting misfolded SOD1 were reported to delay disease onset and increase survival in independent ALS-linked SOD1 mutant mouse models (29). Another study explored the potential of immunotherapy for treating *C9orf72* ALS/FTD by using a mouse-derived antibody against poly-GA in cultured cells (30), and a potential beneficial effect of poly-GA human-derived antibodies was reported in *C9orf72* BAC transgenic mice expressing 500 repeats (31). Most recently, the effect of active immunization against poly-GA (32) was assessed in a mouse model overexpressing poly-GA fused with the cyan fluorescent protein ($(GA)_{149}$-CFP;). Reduction in poly-GA accumulation, neuroinflammation, and TDP-43 mislocalization was observed in $(GA)_{149}$-CFP mice immunized with ovalbumin-$(GA)_{10}$ conjugates (32). Several nonexclusive mechanisms have been proposed for antibody-mediated neutralization of intracellular aggregates. In particular, antibodies to tau or α-synuclein may influence disease progression by inhibiting cell-to-cell propagation of toxic proteins (27, 33), a mechanism proposed also for *C9orf72* DPRs (20, 30, 34). Moreover, several studies suggest that antibodies are internalized by neuronal cells (35, 36), where they may capture accumulated protein aggregates and facilitate their degradation.

Here, we systematically characterized 11 human anti-DPR antibodies generated by immune repertoire analyses of healthy elderly donors and tested poly-GA antibodies in multiple cell lines, including human neuronal cultures and two *C9orf72* mouse models. Poly-GA-specific antibodies entered cultured neurons and colocalized with their target in intracellular vesicles. Moreover, long-term antibody treatment of human neurons expressing poly-GA resulted in capturing of extracellular poly-GA and lead to the formation of extracellular antibody-poly-GA complexes. In transgenic mice expressing the *C9orf72* gene containing 450 G_4C_2 repeats ($C9^{450}$) or in mice expressing 149 G_4C_2 repeats within the central nervous system by means of adeno-associated virus (AAV-G_4C_2) (37, 38), antibodies were shown to cross the blood–brain barrier without obvious adverse effects upon long-term chronic administration. However, in the $(AAV\text{-}G_4C_2)_{149}$ mice, antibody treatment was not efficient in clearing poly-GA aggregates and was associated with increased poly-GA levels measured by immunoassay. While an improvement was observed in one behavioral assay in $C9^{450}$ mice, treatment was not associated with alleviation of disease progression in $(AAV\text{-}G_4C_2)_{149}$ mice.

Results

Antibody Generation and Affinity Determination. Human monoclonal antibodies targeting the five *C9orf72* DPRs were generated by screening memory B cell libraries from healthy elderly subjects, an approach previously used to identify potent antibodies recognizing protein aggregates that include amyloid-β, SOD1, or α-synuclein (23). Eleven antibodies with high affinity to one or multiple DPRs were characterized by ELISA (*SI Appendix*, Table S1 and Fig. S1*A*), biolayer interferometry (*SI Appendix*, Table S1 and Fig. S1*B*), and immunostaining (*SI Appendix*, Table S1 and Figs. S2–S6). Four poly-GA-specific antibodies, designated α-$GA_{1\text{-}4}$, were identified with nanomolar EC_{50} constants (0.2–0.3 nM) (*SI Appendix*, Table S1 and Fig. S1*A*). Kinetic analyses by biolayer interferometry revealed that the four α-GA antibodies had comparable association rate constants (k_a) to GA_{15} peptides. α-$GA_{2\text{-}4}$ showed comparably low dissociation rates (k_d), whereas faster target dissociation was observed for α-GA_1 (*SI Appendix*, Table S1 and Fig. S1*B*). Antibody α-GP_1 displayed high-affinity binding to poly-GP and a 26-fold lower affinity to poly-GA (*SI Appendix*, Table S1 and Fig. S1*A*). By screening against the arginine-rich DPR proteins, poly-GR and poly-PR, we further identified α-PR_2, which exclusively recognized poly-PR (EC_{50} of 12.8 nM), as well as several antibody candidates targeting more than one DPR species, α-$PR_{1,3}$ and α-GR_1. Two candidates with high-affinity EC_{50} binding (0.1–0.4 nM) to poly-PA were identified, with α-PA_1 specifically targeting poly-PA (*SI Appendix*, Table S1 and Fig. S1*A*).

The four human anti-GA (α-$GA_{1\text{-}4}$) and the anti-GP (α-GP_1) antibodies specifically recognized aggregates in human brain tissues from ALS patients carrying pathogenic expansions in the *C9orf72* gene (*SI Appendix*, Table S1 and Fig. S2 *A* and *B*, *Upper* panels) and in transgenic mice expressing 450 *C9orf72* hexanucleotide repeats ($C9^{450}$) (37) (*SI Appendix*, Table S1 and Fig. S2 *A* and *B*, *Lower* panels). Antibodies targeting poly-GR, poly-PR, and poly-PA (α-GR_1, α-$PR_{1\text{-}3}$, and α-$PA_{1,2}$) failed to detect DPR aggregates following immunostaining of formalin-fixed human and mouse tissues (*SI Appendix*, Table S1).

To further test antibody specificity across all five DPRs, we transiently transfected motor neuron-like cells (NSC-34) with single DPR species with 50 repeats and tagged with the enhanced green fluorescent protein (GFP) (*SI Appendix*, Figs. S2–S6). Immunofluorescence analysis revealed a predominantly cytoplasmic, diffuse distribution of GA_{50}-GFP, GP_{47}-GFP, and PA_{50}-GFP, with GA_{50}-GFP also forming dense and bright aggregates. GR_{50}-GFP accumulated either in the cytoplasm or in the nucleus and PR_{50}-GFP localized in nuclei. All four human-derived α-GA antibodies (α-$GA_{1\text{-}4}$) specifically recognized poly-GA, with no cross-reactivity to other DPR species (*SI Appendix*, Table S1 and Figs. S2 *C* and *D* and S3). Specificity of the α-GA antibodies was confirmed by the absence of signals in GFP-only transfected cells and in cells stained with secondary antibody only (*SI Appendix*, Fig. S4*A*). In addition to displaying a strong, specific staining for poly-GP, antibody α-GP_1 also showed a weak reactivity for poly-GA, consistent with its in vitro binding affinity (EC_{50} values in *SI Appendix*, Table S1), as well as a faint nonspecific nuclear staining (*SI Appendix*, Fig. S4*B*). Two α-PA antibodies, α-$PA_{1,2}$, specifically recognized poly-PA (*SI Appendix*, Table S1 and Fig. S5), while antibodies α-$PR_{2,3}$ detected poly-PR in the nucleus, particularly in nucleoli, but no other DPR species (*SI Appendix*, Table S1 and Fig. S6). Since α-GA and α-GP reliably detected aggregates in $C9^{450}$ mouse and *C9ORF72* ALS patient brain sections, we selected α-GA_1, α-GA_3, and α-GP_1 (or murine chimeric IgG2a derivatives of each: ^{ch}α-GA_1, ^{ch}α-GA_3, and ^{ch}α-GP_1) to test their ability to impact poly-GA and poly-GP accumulation in vitro and in vivo.

Antibody Uptake and Colocalization with Poly-GA in Cells. To determine if living cells internalize anti-GA antibodies, human neuroblastoma SH-SY5Y cells were transfected to express either a GFP control construct or GA_{50}-GFP and incubated in media containing antibodies α-GA_1, α-GA_3, or an IgG isotype control (50 nM, 72 h). A strong antibody signal was detected in SH-SY5Y cells expressing GA_{50}-GFP and treated with α-GA_1 or α-GA_3 compared to cells incubated with an IgG control or cells expressing GFP only (*SI Appendix*, Fig. S7 *A* and *B*). This result is consistent with the presence of poly-GA within cells enhancing retention of internalized α-GA human antibodies. Automated quantification confirmed colocalization between GA_{50}-GFP and α-GA antibodies. Indeed, 43% and 55% of GA_{50}-GFP area colocalized with α-GA_1 and α-GA_3, respectively, while less than 2% of the GFP-positive area colocalized with these antibodies ($P < 0.001$; *SI Appendix*, Fig. S7*C*). Importantly, GA_{50}-GFP did not colocalize with the IgG control ($P < 0.001$; *SI Appendix*, Fig. S7*C*). Similar results were obtained when quantifying

the total area of antibodies that colocalized with GFP versus GA_{50}-GFP, with approximately 40% of the α-GA_1 and α-GA_3 signal overlapping with GA_{50}-GFP, while less than 8% overlapped with GFP ($P < 0.001$; *SI Appendix,* Fig. S7*D*).

A flow cytometry-based approach using directly labeled human antibodies (*SI Appendix,* Fig. S8*A*) was used to quantify antibody uptake by SH-SY5Y cells transfected to express HA-GA_{50} or exposed to transfection reagents without any plasmid (mock transfected). After incubation with fluorescently labeled α-GA_1, α-GA_3, or IgG isotype for 24 or 48 h, cells were treated with trypsin and trypan blue before analysis by flow cytometry to ensure that the detected fluorescence corresponds to internalized antibodies (36) (*SI Appendix,* Fig. S8). As seen before with confocal microscopy (*SI Appendix,* Fig. S7), accumulation of poly-GA increased the intracellular α-GA_1 and α-GA_3 antibody signal within 24 (*SI Appendix,* Fig. S8*C*) or 48 h (*SI Appendix,* Fig. S8 *B* and *D*) compared to cells not expressing poly-GA ($P < 0.001$; Fig 1*E* and *SI Appendix,* Fig. S8 *B–F*). Only 2 to 6% of the mock transfected (*SI Appendix,* Fig. S8 *B–D*) or the nontransfected cells (*SI Appendix,* Fig. S8 *E* and *F*) had detectable internalized antibodies while 15 to 22% of poly-GA-transfected cells had internalized α-GA_1 and α-GA_3 antibodies. Notably, internalization of α-GA_3 was more efficient than α-GA_1 with a trend already observed after 24 h of treatment ($P = 0.055$; *SI Appendix,* Fig. S8*C*) and a significant difference after 48 h ($P < 0.001$; *SI Appendix,* Fig. S8*D*). Detectable levels of internalized IgG control were found in less than 9% of the cells in all conditions.

To corroborate these findings, we used an independent, stable, and inducible T98G glioblastoma cellular model overexpressing GA_{161}-GFP. Following treatment with 100 nM α-GA_1 or an IgG control antibody for 72 h, cells were stained with anti-human IgG. Image analysis demonstrated that α-GA_1 colocalized with poly-GA aggregates within T98G cells, while isotype control was not observed within cells (*SI Appendix,* Fig. S9*A*). Treatment of T98G cells with α-GA_1 reduced the number of aggregates per cell by 29% (*SI Appendix,* Fig. S9*B*) and reduced the volume of poly-GA aggregates per cell by 39% (*SI Appendix,* Fig. S9*C*).

Antibody Uptake and Colocalization with Poly-GA in Human Neurons. The enhancement of antibody internalization or retention in presence of poly-GA was also seen in cultured human neurons. Neural stem cells (NSCs) were differentiated for 6 wk into a functional neural networks containing neurons and astrocytes (39) and treated for 72 h with ^{ch}α-GA_3 added to the medium. High-magnification confocal images revealed that ^{ch}α-GA_3 was internalized by human neurons (*SI Appendix,* Fig. S10*A*, *Upper* panels, arrowheads, and *Inset*) with no detectable signal in nontreated cells (*SI Appendix,* Fig. S10*A*, *Lower* panels). Neurons were transduced with a lentivirus expressing doxycycline-inducible GA_{50}-GFP and treated for 72 h with ^{ch}α-GA_1, ^{ch}α-GA_3, or an IgG control (Fig. 1*A* and *SI Appendix,* Fig. S10*B*). Both ^{ch}α-GA_3 and the control antibodies were detected as extracellular clumps and internalized by GA_{50}-GFP-expressing neurons at 72 h of treatment. While intracellular localization of ^{ch}α-GA_3 was observed in almost 100% of GA_{50}-GFP-expressing cells, the IgG control antibody was rarely found accumulated intracellularly (18%, $P < 0.0001$; Fig. 1 *A* and *B*). In contrast with ^{ch}α-GA_3, intracellular ^{ch}α-GA_1 was detected only after 21 d of treatment (*SI Appendix*, Fig. S10*B*). Three-dimensional reconstitution of confocal images of GA_{50}-GFP-expressing human neurons treated with ^{ch}α-GA_3 revealed partial colocalization of GA_{50}-GFP and ^{ch}α-GA_3 (*SI Appendix*, Fig. S10*C*). Notably, we observed an incomplete colocalization of ^{ch}α-GA antibodies with large round intracellular aggregates (*SI Appendix,* Fig. S10*B*, *Inset*), suggesting that the antibodies may not penetrate the dense core of these structures.

To understand the intracellular compartment of the observed antibody–antigen interaction, we performed coimmunostaining of GA_{50}-GFP, ^{ch}α-GA_3, and either RAB7 (endosomes) or LAMP1 (lysosomes). This analysis revealed that GA_{50}-GFP and antibody partially colocalized with each of these markers (Fig. 1*C*), supporting that intracellular interaction between poly-GA and externally delivered antibodies occurred within trafficking vesicles. Of note, the presence of the α-GA antibody was not required for the localization of GA_{50}-GFP into endosomal vesicles (Fig. 1*C*, *Lower* panel). To determine whether the presence of intracellular antibody facilitated the engulfment of GA_{50}-GFP in intracellular vesicles, we quantified the colocalization between approximately 1400 GA_{50}-GFP particles and each of these markers using super-resolution microscopy (Fig. 1 *D* and *E*). Antibody treatment with ^{ch}α-GA_3 showed a trend ($P = 0.08$) in favoring the colocalization of GA_{50}-GFP with late endosomes compared to treatment with the IgG control. Indeed 22% of GA_{50}-GFP vesicles were colocalized with Rab7 in cells treated with ^{ch}α-GA_3 compared to 12.7% in cells treated with the IgG control (Fig. 1*E*). Localization of GA_{50}-GFP in lysosomes was not affected ($P = 0.54$) (Fig. 1*E*).

Taken together, these data demonstrate that α-GA antibodies entered cells and engaged intracellular poly-GA, the presence of which enhanced antibody uptake or intracellular retention. Antibody and GA_{50}-GFP were found in similar intracellular vesicles, with no significant changes of GA_{50}-GFP localization induced by ^{ch}α-GA_3 antibody treatment.

Long-Term Antibody Treatment in Human Neurons Modulates Poly-GA Solubility by Forming Extracellular Immune Complexes. To determine whether chronic antibody treatment can modulate the aggregation state of poly-GA or trigger the aggregate clearance, we added ^{ch}α-GA_1, ^{ch}α-GA_3, or IgG control antibodies to the culture medium of human neural culture transduced with inducible GA_{50}-GFP. After 3, 7, or 21 d of poly-GA induction and simultaneous antibody treatment, cells were either fixed for immunofluorescence imaging followed by aggregate count or lysed for biochemical analysis (Fig. 2*A*). Without antibody addition, only a faint, diffused, or fine punctate GA_{50}-GFP signal was detectable in the cytoplasm 3 d after induction (*SI Appendix,* Fig. S11*A*). By 7 d, GA_{50}-GFP either formed round and bright particles reminiscent of aggregates or less bright and irregularly shaped structures resembling preinclusions (Fig. 2*B* and *SI Appendix,* Fig. S11*A*). At 21 d, both aggregates and preinclusions increased in number (Fig 2*C* and *SI Appendix,* Fig. S11*A*). Quantification confirmed the time-dependent increase of GA_{50}-GFP intracellular inclusions (Fig 2*C*, gray bars), which remained unaffected by the addition of ^{ch}α-GA_1 (Fig. 2*C*) or ^{ch}α-GA_3 (*SI Appendix,* Fig. S11*B*) into the cell culture medium.

Interestingly, the addition of ^{ch}α-GA_1 (Fig. 2 *B* and *D*) and ^{ch}α-GA_3 antibodies (*SI Appendix,* Fig. S11*C*), but not of the IgG control (Fig. 2 *B* and *D*), markedly increased the presence of extracellular bright, large, irregularly shaped GA_{50}-GFP complexes (Fig. 2*B*) which colocalized with ^{ch}α-GA_1 (Fig. 2*E*) or ^{ch}α-GA_3 (*SI Appendix*, Fig. S11*D*). Extracellular antibody-poly-GA complexes were stable for at least 7 d after doxycycline was removed to suppress new GA_{50}-GFP production (Fig. 2*D*). The formation of extracellular immune complexes was consistent with natural release of poly-GA from cells into the medium (34), as cell counting did not reveal poly-GA or antibody-mediated cell death (Fig. 2*F* and *SI Appendix*, Fig. S11*E*).

Biochemical analysis showed that the levels of soluble poly-GA were not different across experimental groups (*SI Appendix,* Fig. S11*F*).

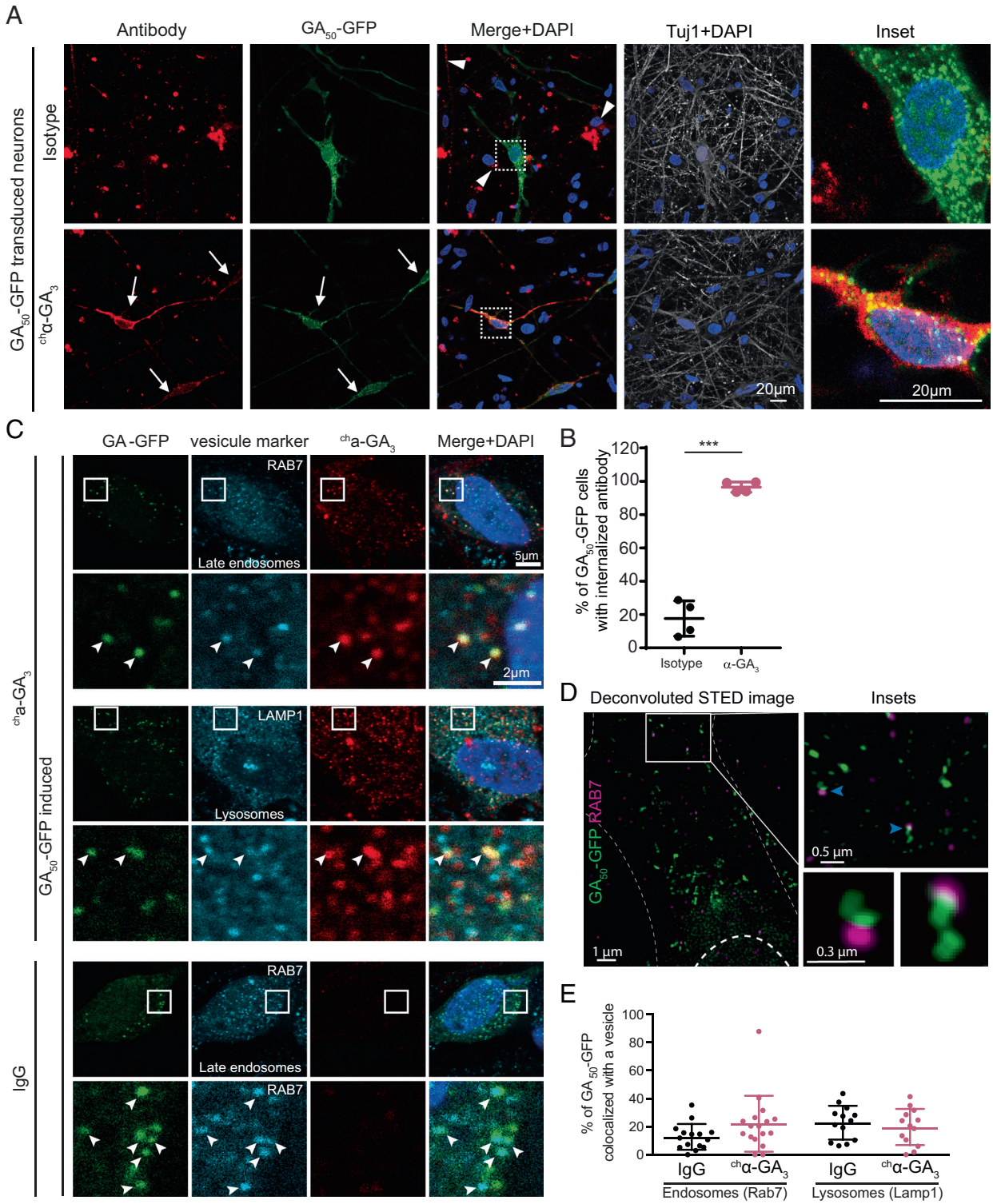

Fig. 1. ^{ch}α-GA$_3$ is internalized *via* vesicular compartments in human neurons, but does not alter GA$_{50}$-GFP vesicular localization. (*A*) Confocal images of human neural cultures expressing inducible GA$_{50}$-GFP, treated for 3 d with ^{ch}α-GA$_3$ or IgG control and stained with a secondary α-human antibody (red). White arrows show antibody/GA$_{50}$-GFP double-positive cells. Arrowheads show antibody uptake in cells not expressing GA$_{50}$-GFP. (Scale, 20 µm.) (*B*) Quantification of the percentage of GA$_{50}$-GFP expressing cells with internalized antibody. Four replicates, unpaired *t* test, *** $P \leq 0.001$. (*C*) Confocal images after staining with either α-RAB7 (late endosomes) or α-LAMP1 (lysosomes). Chimeric antibodies are detected with α-mouse antibody (red). (*D*) Deconvoluted STED image from a neuron expressing GA$_{50}$-GFP treated with ^{ch}α-GA$_3$ and stained with RAB7. *Inset* of the STED image (*Upper* panel) and the created 2D surface (*Lower* panels) are enlarged from the original site (white box). (*E*) The percentage of GA$_{50}$-GFP particles containing a vesicle within a 100 nm radius were considered as colocalized with the indicated vesicle. Each dot represents a field of view. Mann and Whitney *U* test (Rab7 $P = 0.087$ and Lamp1 $P = 0.544$).

On the other hand, poly-GA isolated by detergent solubilization followed by centrifugation (40) and quantified with a filter-retardation assay were markedly increased at all time points in neural cultures incubated with ^{ch}α-GA$_1$ (Fig. 2 *G* and *H*) or ^{ch}α-GA$_3$ (*SI Appendix*, Fig. S11 *G* and *H*) compared with control samples, supporting the presence of poly-GA/antibody immune complexes.

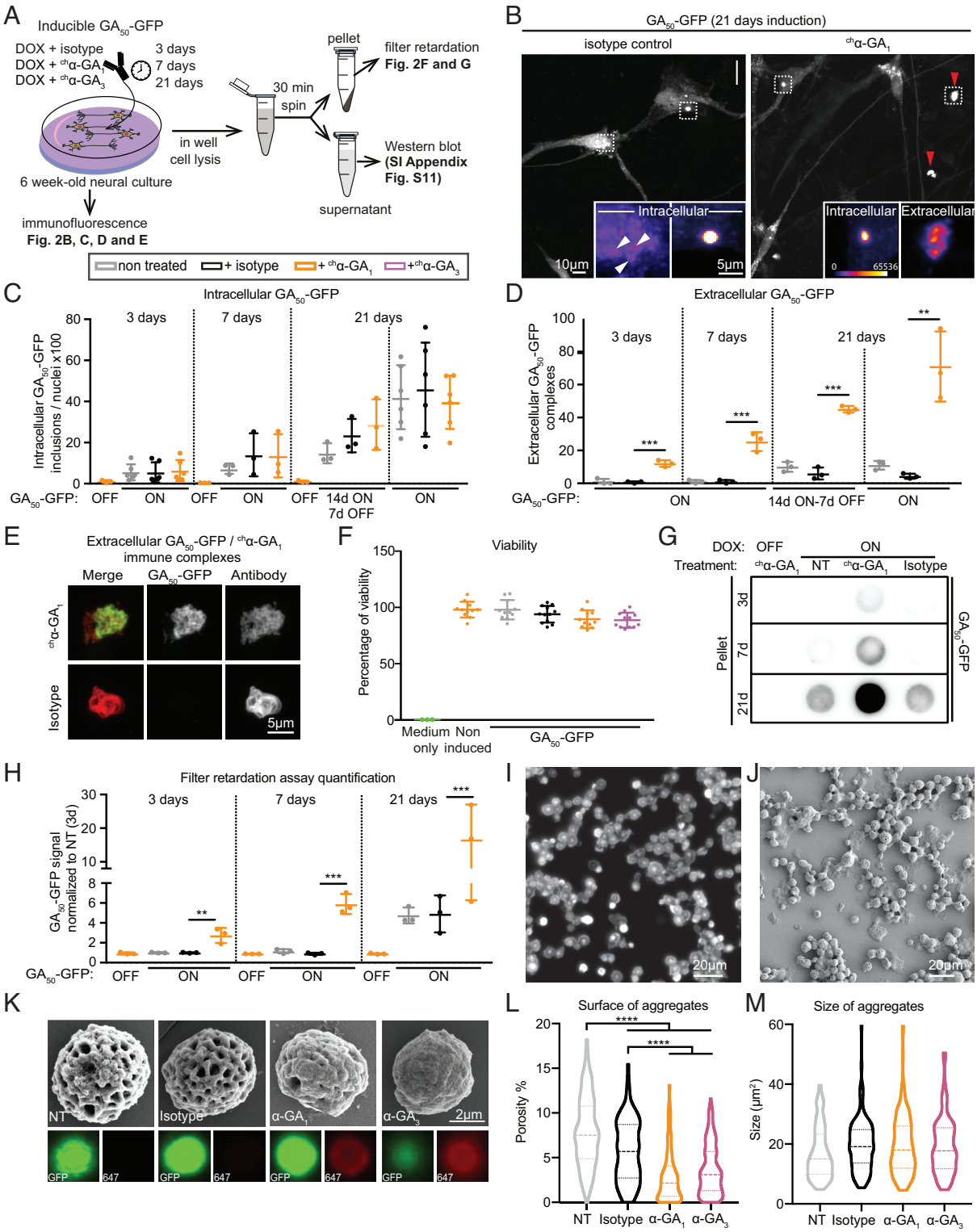

Fig. 2. Poly-GA and antibodies form large heterocomplexes in long-term treated neuronal cultures. (*A*) Experimental strategies to test the effect of antibody treatment on human neurons expressing GA_{50}-GFP. (*B*) Immunofluorescence showing GA_{50}-GFP in neurons treated for 21 d with either an IgG control (*Left* panel) or $^{ch}\alpha$-GA_1 (*Right* panel). The presence of large irregular extracellular GA_{50}-GFP structures only in samples treated with $^{ch}\alpha$-GA_1 antibody (red arrowheads and *Bottom Right Inset*). Insets illustrate different GA_{50}-GFP intracellular structures observed across all conditions, including preinclusions (white arrowheads). (Scale, 10 and 5 µm.) (*C*) Quantification of intracellular GA_{50}-GFP structures normalized to the number of nuclei, 36 images per well, and 3–6 wells per condition. (*D*) Quantification of GA_{50}-GFP extracellular structures normalized to the number of nuclei, 5 images per well, and 3–6 wells per condition. Means +/− SD, beta-binomial test. (*E*) Confocal imaging of an $^{ch}\alpha$-GA_1 extracellular structure colocalizing with GA_{50}-GFP (*Upper* row), and an IgG control extracellular structure, not colocalizing with GA_{50}-GFP (*Lower* row). Antibodies were detected with α-mouse-Alexa 647. (*F*) Cell viability of human neurons expressing GA_{50}-GFP treated with $^{ch}\alpha$-$GA_{1,3}$ or control antibody for 3 d. (*G*) Representative blots and (*H*) quantification of a filter retardation assay for human neurons treated during 3, 7, or 21 d with $^{ch}\alpha$-GA_1 or IgG control. Intensity of each replicate was normalized to the 3 d IgG control samples. Unpaired *t* test is used on the log10(x+1) transformed data. (*I*) Epi-fluorescent image of GA_{50}-GFP aggregates isolated from transiently transfected HEK293T cells. (*J*) Isolated GA_{50}-GFP aggregates visualized via SEM imaging. (*K*) Representative SEM and corresponding IF images of nontreated (NT) or Alexa Fluor 647-labeled IgG control-, α-GA_1-, and α-GA_3-treated GA_{50}-GFP aggregates. (*L* and *M*) Surface porosity (*L*) and total area (*M*) quantifications of the antibody-treated GA_{50}-GFP aggregates. NT n = 139; IgG control n = 125; α-GA_1 n = 183; α-GA_3 n = 193. One-way ANOVA followed by Tukey's test. $P > 0.05$ (no indication), ** $P \leq 0.01$, *** $P \leq 0.001$.

To test whether binding of α-GA antibodies to poly-GA aggregates alters their morphology, we first developed a biochemical method for the purification of GA_{50}-GFP aggregates from transiently transfected HEK293T cells. Extracted GA_{50}-GFP aggregates showed remarkable purity and homogeneity, permitting their characterization via scanning electron microscopy (SEM) (Fig. 2*I*). GA_{50}-GFP-expressing HEK293T cellular extracts were incubated with human Alexa Fluor 647-labeled α-GA_1, α-GA_3, or IgG control antibodies, followed by poly-GA aggregate purification, brightfield, immunofluorescence, and SEM imaging to eventually carry out correlative light-electron microscopy (CLEM) (*SI Appendix,* Fig. S12). We then assessed and quantified the direct effects of antibody binding on the formation of poly-GA aggregates. Untreated or IgG control-treated poly-GA aggregates appeared consistently spherical and with regular surface pores (Fig. 2*K*). In contrast, binding of either α-GA_1 or α-GA_3 antibodies to poly-GA aggregates altered their morphology and yielded aggregates with a smoother surface (Fig. 2 *K* and *L*). Antibody binding had no effect on the size of the poly-GA spheres, which ranged roughly between 10 and 40 μm^2 (Fig. 2*M*). These results indicate that antibody binding directly alters the biochemical and potentially biological properties of GA_{50}-GFP aggregates, which may affect their toxicity and spreading potential.

Overall, antibodies against poly-GA engaged extracellular GA_{50}-GFP into detectable poly-GA/antibody immune complexes, without affecting soluble GA_{50}-GFP levels or poly-GA intracellular structures, while they altered GA_{50}-GFP aggregate formation and morphology in cellular extracts, potentially via stabilization of the poly-GA molecules within the aggregates.

Pharmacokinetics and Brain Penetration of Human-Derived Antibodies Peripherally Administered in $C9^{450}$ Mice. To test the therapeutic potential of antibodies with high affinity and specificity against poly-GA and poly-GP, three antibodies were selected for investigation in two different G_4C_2-expressing mouse models. The pharmacokinetic and antibody brain penetration properties of human-derived α-GA_1, α-GA_3, or α-GP_1 antibodies were determined after a single intraperitoneal (i.p.) injection of 30 mg/kg of antibodies to transgenic mice expressing a human bacterial artificial chromosome (BAC) with 450 G_4C_2 repeats ($C9^{450}$) (37) (*SI Appendix,* Fig. S13 *A–D*). The maximum concentrations (C_{max}) in the plasma were 565 ± 30, 338 ± 24, and 587 ± 54 μg/ml with estimated terminal elimination half-lives ($t_{1/2}$) of 10.8, 11.0, and 7.2 d for α-GA_1, α-GA_3, and α-GP_1, respectively. The corresponding C_{max} in the brain were 0.41 ± 0.16, 0.12 ± 0.07, and 0.28 ± 0.09 μg/mg of total brain protein measured at 2 d postinjection. All antibodies were undetectable by 3 wk post administration. The ratio of the brain drug concentration to the plasma concentration measured at 2 d post injection was 0.05 to 0.1%, consistent with previous reports for systemically administered antibodies (41). Immunofluorescence using human-specific IgG secondary antibodies did not detect α-GA_1, α-GA_3, and α-GP_1 antibodies 10 d after a single i.p. injection in 20-mo-old $C9^{450}$ mouse brains having accumulated poly-GA aggregates (*SI Appendix,* Fig. S13*E*).

Chronic Administration of Human-Derived Antibodies Modulates Poly-GA Solubility without Significantly Altering Poly-GA Levels in $C9^{450}$ Mice. To evaluate the effect of antibodies on the development of DPR pathology in mouse brains, antibodies were intraperitoneally injected in $C9^{450}$ mice from 3 to 19 mo of age (Fig. 3*A*). To circumvent the mouse immune response toward the chronic administration of human antibodies, we used murine IgG2a chimeric derivatives of the human antibodies. Chimeric α-GA antibodies (^{ch}α-GA_1, ^{ch}α-GA_3) and α-GP antibody (^{ch}α-GP_1) were administered once a week at 30 mg/kg in $C9^{450}$ mice starting at 3 mo of age (Fig. 3*A*). Mice from both sexes were randomly assigned to treatment groups and investigators were blinded throughout the studies. The poly-GA aggregate load detectable by immunohistochemistry in $C9^{450}$ mice was too low and variable in this cohort to be reliably quantified. Levels of soluble poly-GA and poly-GP were measured at 7 mo of age by immunoassay after sonication of brain homogenates in the presence of 2% SDS (37) (*SI Appendix,* Fig. S14*A*, fraction 1) from $C9^{450}$ mice expressing comparable levels of the transgene (*SI Appendix,* Fig. S14*B*). Insoluble fractions obtained by ultracentrifugation and resuspension of the corresponding pellet in 7 M urea (*SI Appendix,* Fig. S14*A*, fraction 2) were measured using similar immunoassays. Soluble poly-GP did not significantly differ between treatment groups (*SI Appendix,* Fig. S14*C*). Poly-GA proteins, however, were not detectable in mice treated with ^{ch}α-GA_1 and ^{ch}α-GA_3 and were significantly reduced in mice treated with ^{ch}α-GP_1 (an antibody recognizing poly-GA with lower affinity; *SI Appendix,* Figs. S1*A* and S4*B*) compared to mice injected with saline only (*SI Appendix,* Fig. S14*D*). This observation suggests that α-GA antibodies interfere with the detection of poly-GA in immunoassays that do not include denaturation of the samples, likely by masking of the epitopes by the injected antibody (Fig. 3*B*, *Left* panel). In addition, while poly-GA was normally not detected in the urea-insoluble fraction from saline-injected $C9^{450}$ mice (*SI Appendix,* Fig. S14*E*, $C9^{450}$ PBS), poly-GA was present in the insoluble fraction from mice treated with ^{ch}α-GA_1 or ^{ch}α-GA_3 antibodies (*SI Appendix,* Fig. S14*E*, fraction 2). Notably, similar results were obtained when antibodies were directly spiked into mouse brain homogenates further confirming that poly-GA antibodies form immune complexes with poly-GA that migrate in insoluble fractions and interfere with immunoassay's detection when samples are not efficiently denatured (*SI Appendix,* Fig. S14 *F–H*).

To accurately investigate the effect of antibody treatment on poly-GA levels, we adapted the protocol by denaturing any carry-over antibody that might interfere with the poly-GA immunoassay using resuspension in SDS/tris(2-carboxyethyl)phosphine (TCEP) and boiling of the samples (Fig. 3*B*, *Right* panel, and Fig. 3*C)*. The samples were also subjected to centrifugation and ultracentrifugation after homogenization in 1% TX100 and 0.25% deoxycholate (DOC) (Fig. 3*C*) (31). Denaturation of the brain homogenates demonstrated that poly-GA levels were unchanged between the different treatment groups in the first supernatant fraction (S1) (Fig. 3*D*). Consistent with our previous results (*SI Appendix,* Fig. S14*E*, fraction 2), both ^{ch}α-GA_1 and ^{ch}α-GA_3 i.p. injections in $C9^{450}$ mice increased the presence of poly-GA in the pellet fraction (P2) after ultracentrifugation (Fig. 3*E*), supporting the presence of poly-GA/antibody immune complexes.

Chronic Administration of Human-Derived Antibodies Modulates Poly-GA Solubility and Increases Poly-GA Levels in $AAV(G_4C_2)_{149}$ Mice. The impact of ^{ch}α-GA_1 antibody was also determined in somatic transgenic mice generated by intracerebroventricular (ICV) administration to postnatal day 0 mice of adeno-associated virus encoding either 2 or 149 G_4C_2 hexanucleotide repeats [$AAV(G_4C_2)_2$ or $AAV(G_4C_2)_{149}$] (Fig. 3*F*). Weekly i.p. injections of ^{ch}α-GA_1 or the IgG control were carried out from 2 to 12 mo of age and brains were collected either at 4 or 12 mo of age for poly-GA and poly-GP measurements (Fig. 3 *G–L*). Using an immunoassay that included denaturation of the samples, we identified a significantly increased accumulation of poly-GA in the supernatant S1 fraction in $AAV(G_4C_2)_{149}$ mice treated with

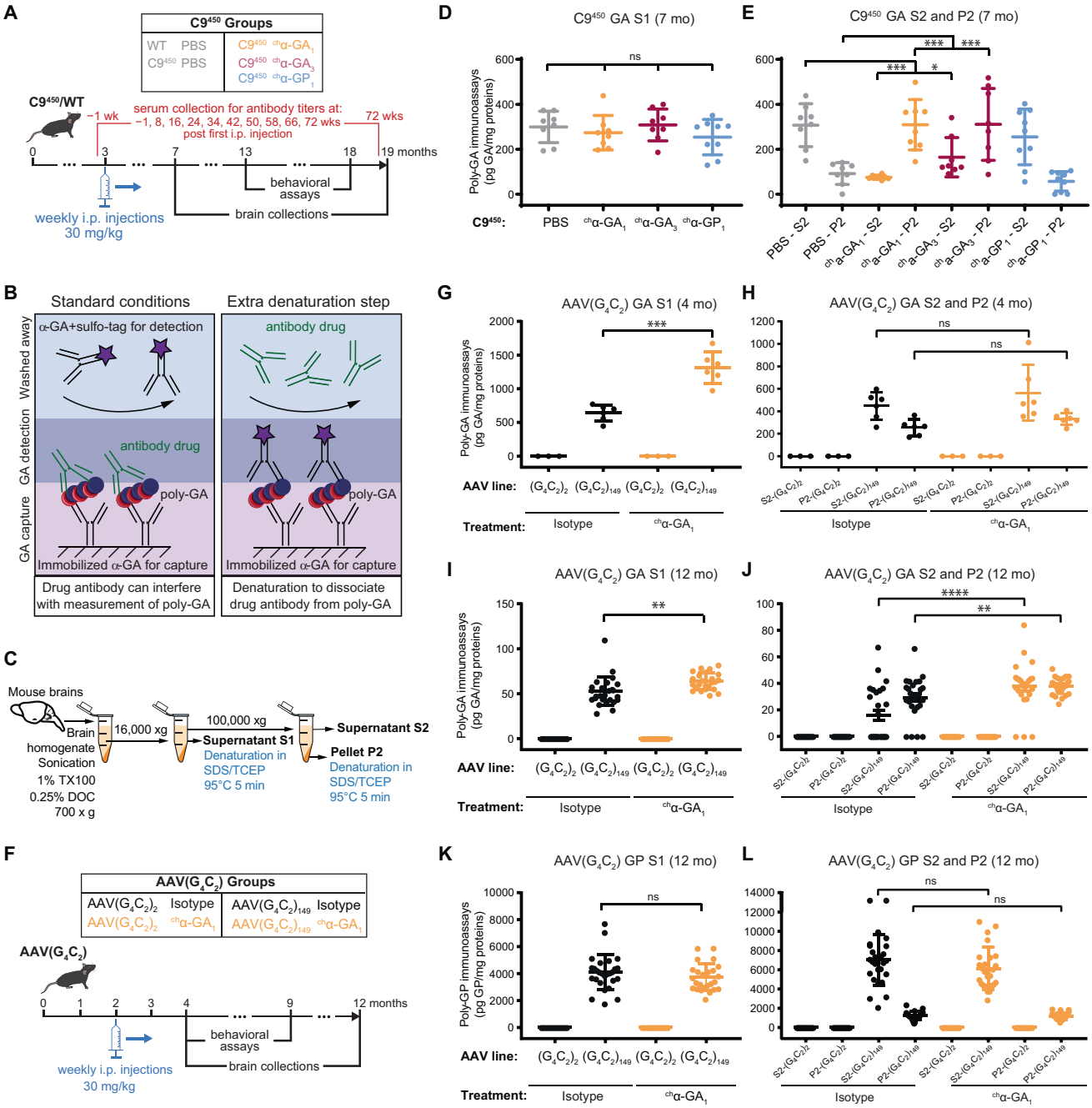

Fig. 3. Immunoassay with sample denaturation identifies elevated levels of poly-GA in brains of mice treated with α-GA antibodies. (*A*) Scheme of chronic antibody treatment in C9^{450} mice receiving intraperitoneal injection of PBS, ^{ch}α-GA$_1$, ^{ch}α-GA$_3$, or ^{ch}α-GP$_1$ antibodies from 3 to 19 mo of age. (*B*) Scheme showing drug–antibody interference in the measurement of poly-GA protein levels using a sandwich-ELISA assay (*Left* panel). The right panel illustrates the effect of sample denaturation prior to measurements. (*C*) Adaptation of a mouse brain fractionation protocol to denature samples and avoid interference of the antibody treatment by ELISA. Fractions highlighted in bold were analyzed. (*D*, *E*) Poly-GA immunoassay from the supernatant S1 (*D*) and after ultracentrifugation (supernatant S2 and pellet P2) (*E*) of brains from 7-mo-old C9^{450} (n ≥ 8 per group). (*F*) Scheme of chronic antibody treatment by intraperitoneal injection of ^{ch}α-GA$_1$ or IgG control to AAV-(G$_4$C$_2$) mice from 2 to 12 mo of age. (*G*–*J*) Poly-GA immunoassay from the supernatant S1 (*G*, *I*) and after ultracentrifugation (supernatant S2 and pellet P2) (*H*, *J*) of brains from AAV-(G$_4$C$_2$) mice at 4 mo (n ≥ 3 per group for AAV-(G$_4$C$_2$)$_2$ and n ≥ 6 for AAV-(G$_4$C$_2$)$_{149}$) (*G*, *H*) and 12 mo (n ≥ 12 per group for AAV-(G$_4$C$_2$)$_2$ and n ≥ 25 for AAV-(G$_4$C$_2$)$_{149}$) (*I*, *J*). (*K*, *L*) Poly-GP immunoassay from the supernatant S1 (*K*) and after ultracentrifugation (supernatant S2 and pellet P2) (*L*) of brains from AAV-(G$_4$C$_2$) mice at 12 mo of age. Mean ± SD, one-way ANOVA followed by Tukey's test. $P > 0.05$ (ns for not significant), ** $P \leq 0.01$, *** $P \leq 0.001$, and **** $P \leq 0.0001$.

^{ch}α-GA$_1$ compared to mice injected with the IgG control at 4 (Fig. 3*G*) and 12 mo (Fig. 3*I*). After ultracentrifugation of the samples, the levels of poly-GA in protein fractions S2 and P2 were not changed at 4 mo of age (Fig. 3*H*) but were significantly increased in all fractions from 12-mo-old mice treated with ^{ch}α-GA$_1$ compared to mice injected with the IgG control (Fig. 3*J*). On the contrary, poly-GP solubility and levels were unaltered by ^{ch}α-GA$_1$ treatment (Fig. 3 *K* and *L*).

In addition, sarkosyl-insoluble pellets isolated via SarkoSpin (40) from total brain homogenates of 4-mo-old AAV(G$_4$C$_2$) mice were analyzed via a filter retardation assay (*SI Appendix*, Fig. S15 *A* and *B*). ^{ch}α-GA$_1$ antibody was specifically retained on the membrane in the ^{ch}α-GA$_1$-treated AAV(G$_4$C$_2$)$_{149}$ mouse samples suggesting that the nondenaturing conditions of the SarkoSpin protocol led to the isolation of sarkosyl-insoluble ^{ch}α-GA$_1$ antibody-poly-GA complexes, which were not observed with IgG

control (*SI Appendix,* Fig. S15 *A* and *B*). Insoluble, poly-ubiquitinated proteins were detected in both AAV$(G_4C_2)_{149}$ mouse conditions, and their levels were not affected by ^{ch}α-GA$_1$ antibody treatment (*SI Appendix,* Fig. S15 *C* and *D*).

Chronic Administration of Human-Derived Antibodies Did Not Impact Poly-GA Aggregate Load in AAV$(G_4C_2)_{149}$ Mice. By 4 mo of age, AAV$(G_4C_2)_{149}$ mice accumulated large perinuclear poly-GA aggregates throughout the brain that colocalized with poly-GR and poly-GP (*SI Appendix,* Fig. S16 *A* and *B*), as observed in postmortem tissues from patients (5). We determined the area occupied by poly-GA aggregates in AAV$(G_4C_2)_{149}$ mice treated for 2 or 10 mo with ^{ch}α-GA$_1$ antibody compared to mice treated with the IgG control. To test whether treatment with α-GA antibodies may interfere with detection of aggregates (as observed in immunoassays without strong denaturation; Fig. 3*B* and *SI Appendix,* Fig. S14 *D* and *G*), immunofluorescence was performed using either an antibody raised against poly-GA (37) or an antibody raised against an N-terminal peptide starting at a CUG initiation codon in the poly-GA frame (8). When using an anti-GA antibody to detect aggregates, there was no change in the poly-GA aggregates after 2 mo of treatment (*SI Appendix,* Fig. S16 *C* and *D*), but the area appeared significantly decreased in the cortex after 10 mo of treatment with ^{ch}α-GA$_1$ antibody (*SI Appendix,* Fig. S16*E*). A nonsignificant similar trend was observed in the hippocampus (*SI Appendix,* Fig. S16*F*). However, this reduction was not observed when we used an antibody raised against the N-terminal peptide of poly-GA (Fig.4 *A* and *B* and *SI Appendix,* Fig. S17 *A* and *B*), demonstrating the importance of using antibodies that recognize different epitopes than the treatment antibody when assessing the effect of an immunotherapy against poly-GA.

As expected, poly-GP aggregates were not affected in either the cortex (*SI Appendix,* Fig. S17*C*, *Left* panels, and *SI Appendix,* Fig. S17*D*) or the hippocampus (*SI Appendix,* Fig. S17*C*, *Right* panels, and *SI Appendix,* Fig. S17*E*). The level of poly-GR measured by immunoassay (*SI Appendix,* Fig. S17*F*) and the area of poly-GR aggregates (*SI Appendix,* Fig. S17*G*) were also not modified by treatment with ^{ch}α-GA$_1$ antibody. Similarly, the number of phospho-TDP-43 aggregates detected by immunohistochemistry in AAV$(G_4C_2)_{149}$ mice was not altered by treatment with ^{ch}α-GA$_1$ (*SI Appendix,* Fig. S17 *H* and *I*).

Long-Term In Vivo Administration of DPR Antibodies Was Well Tolerated with a Modest Impact on Behavior in C9^{450} Mice. C9^{450} mice were treated by weekly injection of ^{ch}α-GA$_1$, ^{ch}α-GA$_3$, and ^{ch}α-GP$_1$ from 3 to 19 mo of age (Fig. 3*A*). Antibody titers in serum (measured every 2 mo, 24 h after injection) remained stable over time (*SI Appendix,* Fig. S18 *A*–*C*). Chronic administration did not result in any obvious adverse effects, with comparable survival (Fig. 4*C*) and body weight (*SI Appendix,* Fig. S18 *D* and *E*) between the different treatment groups, demonstrating the tolerability of all three antibodies at 30 mg/kg per week for 16 mo. At 13 mo of age, only C9^{450} males exhibited a decreased activity with a significant reduction in distance moved compared to age-matched wild-type mice in an open-field assay (*SI Appendix,* Fig. S18*F*). At this age, these differences were not impacted by ^{ch}α-GA$_1$, ^{ch}α-GA$_3$, and ^{ch}α-GP$_1$ antibody treatment (*SI Appendix,* Fig. S18*F*). However, by 18 mo of age, C9^{450} mice treated with PBS continued to display a significantly decreased activity compared to wild-type animals, while mice treated with ^{ch}α-GA$_3$ showed a significant rescue when compared to C9^{450} animals treated with PBS (P = 0.0149) (Fig. 4*D*). Mice treated with ^{ch}α-GA$_1$ and ^{ch}α-GP$_1$ antibodies also showed a nonsignificant trend toward improvement in this behavioral assay (Fig. 4*D*). As previously reported (37), C9^{450} mice develop a loss of hippocampal neurons that was not significantly alleviated by treatment with DPR antibodies (Fig. 4*E*).

Long-Term In Vivo Administration of DPR Antibodies Did Not Significantly Impact Disease Progression in AAV$(G_4C_2)_{149}$ Mice. AAV$(G_4C_2)_{149}$ mice were treated by weekly i.p. injection of ^{ch}α-GA$_1$ at 30 mg/kg from 2 to 12 mo of age (Fig. 3*F*). The survival of these mice was not impacted by the expression of the G_4C_2 repeats as previously described (42), and antibody treatment was well tolerated (Fig. 4*F* and *SI Appendix,* Fig. S18 *G* and *H*). AAV$(G_4C_2)_{149}$ mice presented abnormal activity including increases in distance traveled, velocity of movement and time spent moving on an open-field assay compared to control AAV$(G_4C_2)_2$ mice (Fig. 4 *G*–*I*). These phenotypes were not impacted by chronic administration of ^{ch}α-GA$_1$ antibody. When assessing strength by measuring the ability to cling on an inverted metal grid, female AAV$(G_4C_2)_{149}$ mice showed significantly lower performance compared to AAV$(G_4C_2)_2$ mice (P = 0.002) (Fig. 4*J*). Although there was a trend toward improvement, the deficit in AAV$(G_4C_2)_{149}$ mice was not significantly rescued by ^{ch}α-GA$_1$ treatment (P = 0.11). In addition, treatment with ^{ch}α-GA$_1$ did not impact the decrease in brain weight observed in AAV$(G_4C_2)_{149}$ mice compared to AAV$(G_4C_2)_2$ mice (Fig. 4*K*).

Discussion

In this study, we have characterized potential immunotherapies (based on human antibodies) for *C9orf72*-related ALS and FTD. Eleven antibodies against all five *C9orf72* DPR species were identified and systematically characterized. The exact trigger(s) leading to the production of antibodies against DPRs in healthy people is unknown. It is conceivable that due to their highly repetitive sequences, DPRs may present sequence or structural similarities with other antigens potentially derived from bacteria or viruses. Alternatively, the 2 to 30 (G_4C_2) repeats found in the normal population may produce DPR proteins at a very low rate, which may trigger an antibody-mediated immune response without being pathogenic. While we have systematically characterized antibodies against each *C9orf72*-related DPR, we focused on antibodies against poly-GA, recognizing that this DPR is the most abundant with high aggregation propensity in ALS/FTD human autopsy brain samples (5, 43) and with strong neurotoxicity in mice (18, 21). Moreover, poly-GA has the ability to trap other DPR species and modulate C9ORF72 toxicity observed in multiple cellular and animal models (19, 20, 22).

While antibody treatment against intracellular tau and α-synuclein are currently being tested for Alzheimer's and Parkinson's diseases respectively (26, 27, 33), the exact mechanisms of action of immunotherapy against intracellular proteins remain unclear. Antibodies were shown to either facilitate clearance of the target or to prevent spreading and toxicity. The tested α-GA antibodies were robustly internalized by poly-GA-expressing human neurons, a finding in line with published studies showing antibody uptake by neuronal cells (35, 36). In this cellular model, intracellular antibodies colocalized with poly-GA in cytoplasmic puncta, however, less prominently to very dense and large intracellular aggregates formed over time. It is possible that their compact structure may conceal the epitope recognized by the antibody. Alternatively, poly-GA physical associations with other proteins may interfere with epitope recognition. Antibody and poly-GA colocalized partially with late-endosomes and lysosomes, but anti-GA antibody

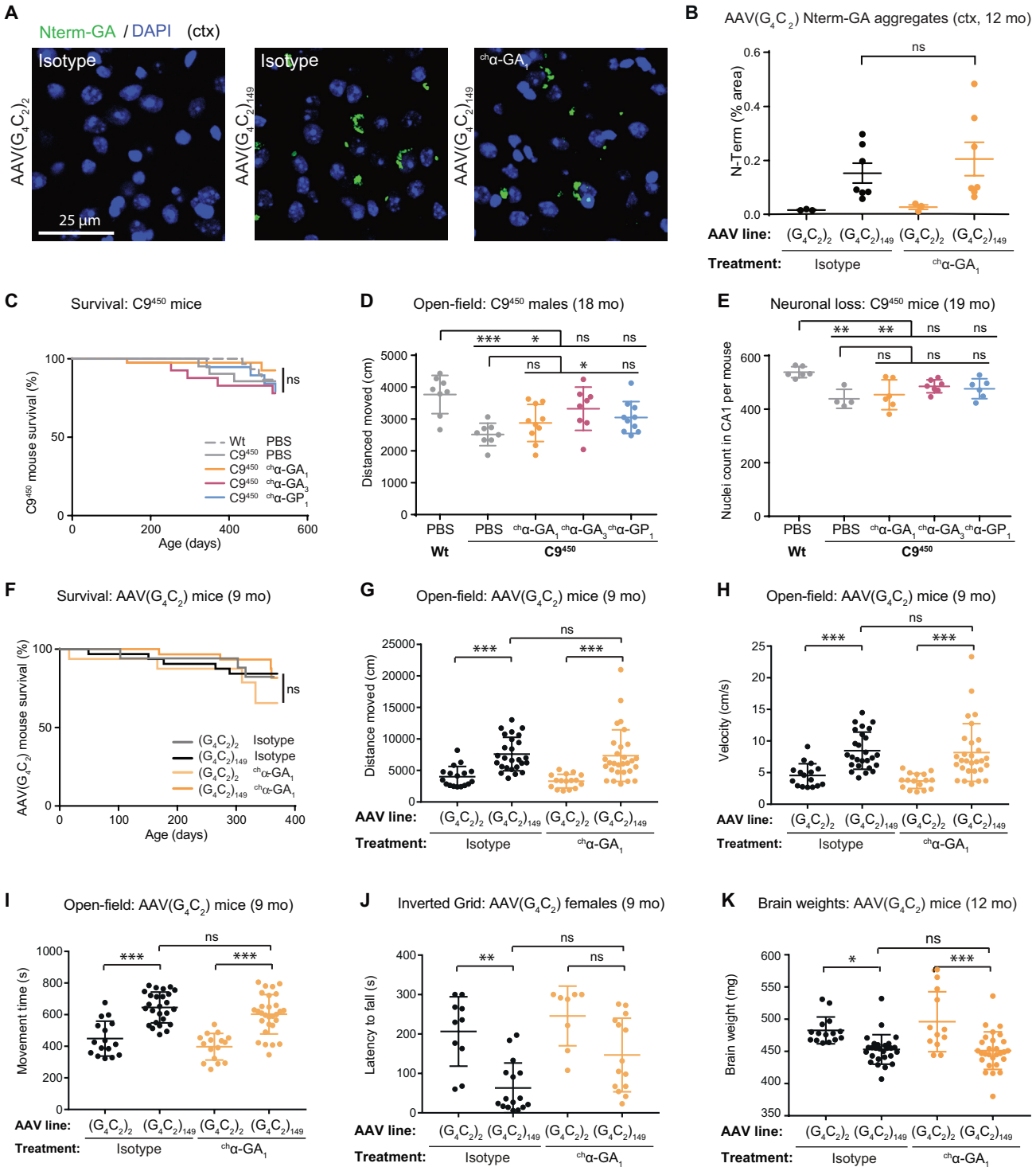

Fig. 4. Chronic administration of α-GA antibodies did not reduce poly-GA aggregates load and impacted only a subset of phenotypes in one of two *C9orf72* mouse models. (*A*) Immunofluorescence of poly-GA in the motor cortex of 12-mo-old AAV-(G_4C_2) mice treated with ^{ch}α-GA_1 or IgG control. (*B*) Percent area occupied by poly-GA aggregates detected with an N-terminal-poly-GA antibody in the cortex (n ≥ 3 per group for AAV-$(G_4C_2)_2$ and n ≥ 7 for AAV-$(G_4C_2)_{149}$). (Scale, 25 µm.) Mean ± SD, one-way ANOVA followed by Tukey's test. (*C*) Survival Kaplan–Meier curves of $C9^{450}$ and wild-type mice receiving injections of PBS, ^{ch}α-GA_1, ^{ch}α-$GA_3$and ^{ch}α-GP_1 antibodies for 16 mo. (*D*) Distance traveled in the open-field by 18-mo-old males (n ≥ 8 per group). Mean ± SD, Kruskal–Wallis test followed by Dunnett's test. (*E*) Nuclei quantification in the hippocampal CA1 region in 19-mo-old mice (n ≥ 4 mice per group; n ≥ 3 matched sections per mouse). Mean ± SD, one-way ANOVA followed by Dunnett's test. (*F*) Survival Kaplan–Meier curve of AAV-(G_4C_2) mice receiving injections of ^{ch}α-GA_1 or IgG control for 10 mo. (*G–I*) Distance traveled (*G*), velocity of movement (*H*) and time spent moving (*I*) in the open-field (n ≥ 16 per group for AAV-$(G_4C_2)_2$ and n ≥ 24 for AAV-$(G_4C_2)_{149}$). (*J*) Time taken to fall from inverted grid by 9-mo-old AAV-(G_4C_2) female mice (n ≥ 8 per group). (*K*) Brain weights of AAV-(G_4C_2) mice treated for 10 mo. Mean ± SD, one-way ANOVA followed by Dunnett's test. $P > 0.05$ (no indication or ns for not significant), * $P \leq 0.05$, ** $P \leq 0.01$, *** $P \leq 0.001$.

treatment did not significantly alter GA_{50}-GFP vesicular localization. Whether antibody and antigen entered the same degradation pathway independently, or antibody binding on poly-GA triggered its engulfment in endocytic vesicles, thereby potentially stimulating its clearance remains unanswered. It is also possible that the antibodies engaged the poly-GA extracellularly and entered human

neurons already as a complex. However, the absence of antibody-engaged poly-GA in nontransduced, wild-type neurons present in the same neuronal network challenges that notion. Rather, as supported by super-resolution microscopy, the dense GA_{50}-GFP inclusions and aggregates may be present in a different compartment than the antibody-engaged poly-GA. Notably, despite target engagement in our cellular models and reduction of poly-GA aggregates in T98G anchorage-independent cancer cell line, intracellular GA_{50}-GFP inclusions and aggregates were not affected by antibody treatment in cultured human neurons, highlighting differences between cell types.

Of note, the three cellular models used in this study were differently modified to overexpress poly-GA. While the liposome-mediated transfection of SH-SY5Y cells may have indirectly enhanced the antibody "uptake" because of the partially compromised cell membrane, both the T98G cells (stable transfection) and human neurons (lentivirus-mediated gene delivery and cell recovery for several days before antibody treatment) likely had an intact cell membrane and thus accurately modeled antibody uptake and/or retention in cancer cells or human neurons, respectively. Interestingly, anti-GA antibodies did engage less prominently the dense poly-GA aggregates in human neurons synthesizing poly-GA, compared to their targeting of aggregates in stably transfected T98G cancer cells. This points to a distinct aggregate handling between cycling cells and differentiated neurons. In addition, IF experiments with fixed and permeabilized motor neuron-like NSC-34 cells overexpressing poly-GA via transient transfection revealed that all tested anti-GA antibodies (α-$GA_{1\text{-}4}$) only partially recognized dense poly-GA aggregates.

It was previously shown that poly-GA is released into the extracellular space and can be taken up by neighboring cells, thereby increasing DPR aggregation (20, 30, 34). A similar mechanism may account for spreading of DPR pathology throughout the nervous system, as was hypothesized for other intracellular protein aggregates found in ALS/FTD (44), a process that may be blocked by immunotherapy. We showed that human-derived antibodies efficiently captured extracellular poly-GA over the course of 3 wk forming large immune complexes in human neuronal cultures. This was also described in the context of Alzheimer's disease, where an anti-tau antibody blocked toxicity and spreading through the formation of immune complexes (45). We were unable to assess whether the formation of poly-GA/antibody immune complexes could rescue poly-GA toxicity in this cellular system since we found no detectable poly-GA toxicity within the time course of 21 d.

In contrast to previous studies that reported a decrease in intracellular aggregates and insolubility of poly-GA upon α-GA treatment in cells (30, 31), our analysis in cultured human neurons did not find a decrease of intracellular inclusions and showed a significant increase of poly-GA insolubility, likely due to the formation of immune complexes (Fig. 2). Antibody-induced insolubility has been previously reported for α-synuclein, which formed amorphous aggregates in vitro in the presence of four out of six tested α-synuclein antibodies (46). In comparison to α-synuclein, which has a strong ability to form fibrils (46), the unusually high hydrophobic and low complexity nature of poly-GA (5, 13) may make it more prone to clump into amorphous aggregates when molecules are brought into close proximity following antibody binding. An antibody selective for soluble tau triggered the formation of extracellular complexes and protected against exogenous paired helical filament toxicity, while an alternative antibody directed against aggregated tau failed at forming extracellular immune complexes and could not confer cellular protection (45).

We also observed that the detection of poly-GA either by immunoassay or by immunofluorescence staining was altered by treatment with α-GA antibodies. Indeed, using an antibody that does not recognize the poly-GA epitopes but rather an N-terminal peptide translated in frame with poly-GA (8), we demonstrated that poly-GA aggregates were not affected by 9 mo of $^{ch}\alpha$-GA_1 treatment in AAV$(G_4C_2)_{149}$ mice (Fig. 4). However, the aggregate load appeared reduced when immunostaining was performed using an antibody against poly-GA (*SI Appendix,* Fig. S16*E*), suggesting that the treatment with $^{ch}\alpha$-GA_1 antibody may block the recognition of poly-GA epitopes by the detecting antibody leading to an underestimation of poly-GA aggregates. The vast majority, if not all, of poly-GA is translated from a start codon located 24 nucleotides upstream of the repeat that encode the N-terminal peptide (8, 47). Hence, it is unlikely that the poly-GA species detected by the N-terminal peptide directed-antibody represent only a subset of poly-GA that would be differently impacted by the treatment. In addition, an interference between the treatment and detection antibodies was demonstrated in a biochemical assay lacking efficient denaturation of the samples before poly-GA measurement (*SI Appendix,* Fig. S14). Such an interference was not observed for the uncharged, flexible, and highly soluble (48) poly-GP molecules (*SI Appendix,* Fig. S14*C*), suggesting that intrinsic structural features of poly-GA are altered by antibody recognition, as supported by our SEM analysis of purified poly-GA (Fig. 2 *I*–*M*). Combined with the robust formation of poly-GA-antibody complexes evident in all our cellular work, these changes highlight the necessity of analyzing all biochemical fractions when comparing antibody-treated to nontreated conditions. While the interference between the treatment and detecting antibodies or antibody-induced biochemical changes may not be an issue for all proteins, our study demonstrates that careful denaturation of biochemical samples and use of antibodies recognizing independent epitopes is warranted for accurate assessment of the impact of immunotherapies on aggregation-prone proteins.

In this study, we have not observed a reversal of the clinical phenotypes linked to *C9orf72* disease in our AAV$(G_4C_2)_{149}$ mice (42) despite starting antibody treatment before onset. This is contrary to a recently published study in a *C9orf72* BAC model (31). The reason for this discrepancy in response to the antibody treatment is unknown—one possibility is that the mouse models used in the two studies display different lengths of the repeat and different phenotypes resulting in distinct responses to antibody treatment. Alternatively, the discrepancy may be linked to the fact that in contrast to other described mouse models expressing G_4C_2 *C9orf72* repeats (37, 38, 42, 49, 50), the model used in the Nguyen et al. study has been reported to develop severe neurodegeneration (31). Notably, Mordes et al. (51) described two independent cohorts of the same model that had similar levels of DPRs but did not have the same behavioral phenotypes previously reported in these mice. While independent laboratories reproduced the originally reported phenotypes in the *C9orf72* BAC mouse model (52), Mordes and colleagues (51) proposed that the severe neurodegeneration reported in a fraction of the mice used by Nguyen and colleagues may be linked to the space cadet syndrome (SCS), previously reported in WT mice with an FVB/N background (53). While *C9orf72*-linked neurodegeneration may be exacerbated by—and potentially distinguished from—the severe seizure phenotypes affecting both *C9orf72* and nontransgenic animals (52), future studies are necessary to determine the relative contribution(s) of the *C9orf72* repeat expansion, the DPR expression levels, and the SCS-linked pathologies to

the described phenotypes and their immunotherapy-driven reversal in different mouse models.

In the current study, we have not observed target engagement by IHC in the brains of our $C9^{450}$ antibody-treated mice despite exchanging protocols and reagents with Dr. Nguyen and colleagues. We have observed constant antibody plasma titers over 1.5 years with brain penetration of a small fraction (~0.1%) of the injected antibody (as previously shown in refs. 41 and 54 for other antibodies), but peripherally injected human antibodies were not found to colocalize with neuronal poly-GA aggregates (*SI Appendix,* Fig. S11*E*). The reason for this difference from the observations in Nguyen et al. (31) is unclear, but it is conceivable that the severe neurodegeneration and/or SCS pathology in the mice used by Nguyen et al. may be associated with blood–brain barrier leakage, which might facilitate antibody entry to the brain. Whether that accounts for the reported decrease in poly-GA load in these mice remains to be clarified. Brain penetration following peripheral administration of antibodies is likely a limiting factor in immunotherapy. Notably, aducanumab, which showed effective target clearance, was reported to have a brain:plasma ratio of 1.3% (23), higher than the 0.1% observed in this study and others (23, 41, 54). Alternative delivery paradigms, including higher and more frequent doses, intracerebroventricular delivery of recombinant antibodies, or AAV-mediated expression of single-chain antibodies should be evaluated in future studies.

In our $C9^{450}$ cohort, the levels of poly-GA and poly-GP could be measured by immunoassay, but the number of poly-GA aggregates was too low to evaluate the effect of antibody treatment on poly-GA aggregate load. Despite the lack of widespread poly-GA pathology, long-term treatment with anti-GA antibodies improved an open-field movement test in aged $C9^{450}$ mice (albeit modestly). In $AAV(G_4C_2)_{149}$ mice, anti-GA treatment failed to ameliorate brain atrophy and poly-GA levels increased following treatment during 9 mo. This finding supports that at least a small portion of peripherally injected antibodies accessed poly-GA in the brain and impacted its turnover. Targeting some of the other reportedly toxic DPR proteins, such as poly-GR and poly-PR, may be an alternative and potentially synergistic approach to treat *C9orf72* disease which should be explored in future studies. Furthermore, we anticipate that antibody delivery is key for the success of immunotherapy and approaches to increase antibody penetration to the central nervous system (55) might result in enhanced therapeutic benefits.

Materials and Methods

All studies in mice were approved by the Massachusetts General Hospital Institutional Animal Care and Use Committee (IACUC). Methods used for production and in vitro characterization of antibodies, cell cultures, immunofluorescence, immunoassays, electron microscopy, and biochemical analyses are available in *SI Appendix*, Materials and Methods.

Data, Materials, and Software Availability. Data, constructs, and reagents generated in this study are all available without restriction with the exception of the human antibodies against dipeptide repeat proteins that require agreement with the industry collaborators.

ACKNOWLEDGMENTS. We thank Moritz Kirshmann and Joe Weber for the support in data analysis, Ulrich Wagner for statistical analysis, Nicola Bothwick, Moaz Abdelrehim, and Mohamed Al Abdulla for technical help, and all the members of the Albers, Wainger, and Aguzzi laboratories for helpful discussions. We are grateful to Asvin Lankkaraju in Adriano Aguzzi's laboratory for providing antibodies. Imaging and analysis was performed at the Center for Microscopy with assistance from Johannes Riemann and Andres Kaech (University of Zurich). Postmortem tissues were obtained from the Massachusetts Alzheimer's Disease Research Center (PG50 AG005134). This work was supported by grants from the ALS Association and NINDS/NIH (R01NS087227) to C.L.-T. and from Target ALS to C.L.-T. and M.P. Researchers were supported by the following fellowships: from the University of Zurich (K-74423-04-01; FK-15-097) to M.J. and M.H.-P., the Swiss National Science Foundation (51NF40-141735) to M.J., the Philippe Foundation to R.T., the ECOR Tosteson Fellowship to F.F., the Milton Safenowitz Postdoctoral Fellowship (16-PDF-247), and the Promotor-Stiftung from the Georges and Antoine Claraz Foundation to M.H.-P.

Author affiliations: [a]Department of Neurology, The Sean M. Healey and AMG Center for ALS at the Massachusetts General Hospital and Harvard Medical School, Boston, MA 02114; [b]Broad Institute of Harvard and MIT, Cambridge, MA 02142; [c]Department of Quantitative Biomedicine, University of Zurich, Zurich, CH-8057 Switzerland; [d]Neurimmune AG, Schlieren, CH-8952 Switzerland; [e]Institute for Regenerative Medicine, University of Zurich, CH-8952 Schlieren, Switzerland; [f]Department of Neuroscience, Mayo Clinic, Jacksonville, FL 32224; [g]Ludwig Institute for Cancer Research, University of California San Diego, La Jolla, CA 92093; and [h]Biogen, Cambridge, MA 02142

Author contributions: M.J., K.D.M., M.H.-P., R.T., F.M., J.G., M.P., and C.L.-T. designed research; M.J., K.D.M., M.H.-P., R.T., C.-Z.L., A.R.-S., C.A., K.S., N.M., N.C., P.B., C.-C.L., X.J., J.P., S.N., Y.G., S.D., I.D.-L., Z.M., J.W., M.W., M.M.D., and T.G. performed research; K.J.-W., J.J., F.F., N.L., P.D.R., M.P.-B., L.M.D., E.B., Y.-J.Z., J.B., B.J.W., M.W.K., M.R., C.H., R.M.N., D.W.C., and L.P. contributed new reagents/analytic tools; M.J., K.D.M., M.H.-P., R.T., C.-Z.L., A.R.-S., C.A., K.S., D.W.C., T.G., F.M., M.P., and C.L.-T. analyzed data; and M.J., K.D.M., M.H.-P., R.T., A.R.-S., L.P., F.M., J.G., M.P., and C.L.-T. wrote the paper.

Reviewers: K.H.F., National Institute of Neurological Disorders and Stroke Intramural Research Program; and H.T.O., University of Minnesota, Medical School.

Competing interest statement: The authors declare a competing interest. K.D.M., N.C., P.B., C.H., R.M.N., F.M., and J.G. are employees of Neurimmune and S.N., Y.G., S.D., I.D.-L., M.W.K., and M.R. are employees of Biogen.

1. A. Renton *et al.*, A hexanucleotide repeat expansion in *C9orf72* is the cause of chromosome 9p21-linked Als-Ftd. *Neuron* **72**, 257–268 (2011).
2. M. DeJesus-Hernandez *et al.*, Expanded Ggggcc hexanucleotide repeat in noncoding region of *C9orf72* causes chromosome 9p-linked Ftd and Als. *Neuron* **72**, 245–256 (2011).
3. J. P. Taylor, R. H. Brown Jr., D. W. Cleveland, Decoding als: From genes to mechanism. *Nature* **539**, 197–206 (2016).
4. P. E. Ash *et al.*, Unconventional translation of *C9orf72* Ggggcc expansion generates insoluble polypeptides specific to C9ftd/Als. *Neuron* **77**, 639–646 (2013).
5. K. Mori *et al.*, The *C9orf72* Ggggcc repeat is translated into aggregating dipeptide-repeat proteins in Ftld/Als. *Science* **339**, 1335–1338 (2013).
6. T. Zu *et al.*, Non-Atg-initiated translation directed by microsatellite expansions. *Proc. Natl. Acad. Sci. U.S.A.* **108**, 260–265 (2011).
7. T. F. Gendron *et al.*, Antisense transcripts of the expanded *C9orf72* hexanucleotide repeat form nuclear RNA foci and undergo repeat-associated Non-Atg translation in C9ftd/Als. *Acta Neuropathol.* **126**, 829–844 (2013).
8. R. Tabet *et al.*, CUG Initiation and frameshifting enable production of dipeptide repeat proteins from ALS/FTD *C9orf72* Transcripts. *Nat. Commun.* **9**, 152 (2018).
9. W. Cheng *et al.*, *C9orf72* Ggggcc repeat-associated non-aug translation is upregulated by stress through Eif2alpha phosphorylation. *Nat. Commun.* **9**, 51 (2018).
10. T. F. Gendron *et al.*, Cerebellar C9ran proteins associate with clinical and neuropathological characteristics of *C9orf72* repeat expansion carriers. *Acta Neuropathol.* **130**, 559–573 (2015).
11. D. M. Mann *et al.*, Dipeptide repeat proteins are present in the P62 positive inclusions in patients with frontotemporal lobar degeneration and motor neurone disease associated with expansions in *C9orf72*. *Acta Neuropathol. Commun.* **1**, 68 (2013).
12. S. Al-Sarraj *et al.*, P62 Positive, Tdp-43 negative, neuronal cytoplasmic and intranuclear inclusions in the cerebellum and hippocampus define the pathology of *C9orf72*-linked Ftld and Mnd/Als. *Acta Neuropathol.* **122**, 691–702 (2011).
13. I. Kwon *et al.*, Poly-dipeptides encoded by the *C9orf72* repeats bind nucleoli, impede rna biogenesis, and kill cells. *Science* **345**, 1139–1145 (2014).
14. S. Mizielinska *et al.*, *C9orf72* repeat expansions cause neurodegeneration in drosophila through arginine-rich proteins. *Science* **345**, 1192–1194 (2014).
15. K. H. Lee *et al.*, *C9orf72* dipeptide repeats impair the assembly, dynamics, and function of membrane-less organelles. *Cell* **167**, 774–788.e17 (2016).
16. K. Y. Shi *et al.*, Toxic Prn poly-dipeptides encoded by the *C9orf72* repeat expansion block nuclear import and export. *Proc. Natl. Acad. Sci. U.S.A.* **114**, E1111–E1117 (2017).
17. Y. Lin *et al.*, Toxic Pr poly-dipeptides encoded by the *C9orf72* repeat expansion target Lc domain polymers. *Cell* **167**, 789–802.e12 (2016).
18. Y. J. Zhang *et al.*, *C9orf72* Poly(Ga) aggregates sequester and impair Hr23 and nucleocytoplasmic transport proteins. *Nat. Neurosci.* **19**, 668–677 (2016).
19. Q. Guo *et al.*, In situ structure of neuronal *C9orf72* poly-Ga aggregates reveals proteasome recruitment. *Cell* **172**, 696–705.e612 (2018).
20. Y. J. Chang, U. S. Jeng, Y. L. Chiang, I. S. Hwang, Y. R. Chen, The glycine-alanine dipeptide repeat from *C9orf72* hexanucleotide expansions forms toxic amyloids possessing cell-to-cell transmission properties. *J. Biol. Chem.* **291**, 4903–4911 (2016).
21. K. D. LaClair *et al.*, Congenic expression of poly-Ga but not poly-Pr in mice triggers selective neuron loss and interferon responses found in *C9orf72* Als. *Acta Neuropathol.* **140**, 121–142 (2020).
22. D. L. Brody, D. M. Holtzman, Active and passive immunotherapy for neurodegenerative disorders. *Annu. Rev. Neurosci.* **31**, 175–193 (2008).

23. J. Sevigny *et al.*, The antibody aducanumab reduces abeta plaques in alzheimer's disease. *Nature* **537**, 50–56 (2016).
24. J. O. Rinne *et al.*, 11c-Pib pet assessment of change in fibrillar amyloid-beta load in patients with Alzheimer's disease treated with bapineuzumab: A phase 2, double-blind, placebo-controlled, ascending-dose study. *Lancet Neurol.* **9**, 363–372 (2010).
25. K. V. Kastanenka *et al.*, Immunotherapy with aducanumab restores calcium homeostasis in Tg2576 Mice. *J. Neurosci.* **36**, 12549–12558 (2016).
26. A. Boutajangout, D. Quartermain, E. M. Sigurdsson, Immunotherapy targeting pathological tau prevents cognitive decline in a new tangle mouse model. *J. Neurosci.* **30**, 16559–16566 (2010).
27. K. Yanamandra *et al.*, Anti-tau antibodies that block tau aggregate seeding in vitro markedly decrease pathology and improve cognition in vivo. *Neuron* **80**, 402–414 (2013).
28. E. Masliah *et al.*, Effects of alpha-synuclein immunization in a mouse model of Parkinson's disease. *Neuron* **46**, 857–868 (2005).
29. M. Maier *et al.*, A human-derived antibody targets misfolded sod1 and ameliorates motor symptoms in mouse models of amyotrophic lateral sclerosis. *Sci. Transl. Med.* **10**, eaah3924 (2018).
30. Q. Zhou *et al.*, Antibodies inhibit transmission and aggregation of *C9orf72* poly-Ga dipeptide repeat proteins. *EMBO Mol. Med.* **9**, 687–702 (2017).
31. L. Nguyen *et al.*, Antibody therapy targeting ran proteins rescues C9 Als/Ftd phenotypes in *C9orf72* mouse model. *Neuron* **105**, 645–662.e611 (2020).
32. Q. Zhou *et al.*, Active poly-Ga vaccination prevents microglia activation and motor deficits in a *C9orf72* mouse model. *EMBO Mol. Med.* **12**, e10919 (2020).
33. H. T. Tran *et al.*, Alpha-synuclein immunotherapy blocks uptake and templated propagation of misfolded alpha-synuclein and neurodegeneration. *Cell Rep.* **7**, 2054–2065 (2014).
34. T. Westergard *et al.*, Cell-to-cell transmission of dipeptide repeat proteins linked to *C9orf72*-Als/Ftd. *Cell Rep.* **17**, 645–652 (2016).
35. E. E. Congdon, J. Gu, H. B. Sait, E. M. Sigurdsson, Antibody uptake into neurons occurs primarily via clathrin-dependent fcgamma receptor endocytosis and is a prerequisite for acute tau protein clearance. *J. Biol. Chem.* **288**, 35452–35465 (2013).
36. G. Gustafsson *et al.*, Cellular uptake of alpha-synuclein oligomer-selective antibodies is enhanced by the extracellular presence of alpha-synuclein and mediated via Fcgamma receptors. *Cell Mol. Neurobiol.* **37**, 121–131 (2017).
37. J. Jiang *et al.*, Gain of toxicity from Als/Ftd-linked repeat expansions in *C9orf72* is alleviated by antisense oligonucleotides targeting Ggggcc-containing Rnas. *Neuron* **90**, 535–550 (2016).
38. J. Chew *et al.*, *C9orf72* repeat expansions in mice cause Tdp-43 pathology, neuronal loss, and behavioral deficits. *Science* **348**, 1151–1154 (2015).
39. M. Hruska-Plochan, Human neural networks with sparse Tdp-43 pathology reveal Nptx2 Misregulation in Als/Ftld. bioXriv [Preprint] (2021). 10.1101/2021.12.08.471089. Accessed 9 December 2021.
40. F. Laferriere *et al.*, Tdp-43 extracted from frontotemporal lobar degeneration subject brains displays distinct aggregate assemblies and neurotoxic effects reflecting disease progression rates. *Nat. Neurosci.* **22**, 65–77 (2019).
41. Y. Levites *et al.*, Insights into the mechanisms of action of anti-abeta antibodies in Alzheimer's disease mouse models. *FASEB J.* **20**, 2576–2578 (2006).
42. J. Chew *et al.*, Aberrant deposition of stress granule-resident proteins linked to *C9orf72*-associated Tdp-43 proteinopathy. *Mol. Neurodegener* **14**, 9 (2019).
43. I. R. Mackenzie *et al.*, Quantitative analysis and clinico-pathological correlations of different dipeptide repeat protein pathologies in *C9orf72* mutation carriers. *Acta Neuropathol.* **130**, 845–861 (2015).
44. M. Polymenidou, D. W. Cleveland, The seeds of neurodegeneration: Prion-like spreading in Als. *Cell* **147**, 498–508 (2011).
45. E. E. Congdon *et al.*, Affinity of tau antibodies for solubilized pathological tau species but not their immunogen or insoluble tau aggregates predicts in vivo and ex vivo efficacy. *Mol. Neurodegener* **11**, 62 (2016).
46. C. Sahin *et al.*, Antibodies against the C-terminus of alpha-synuclein modulate its fibrillation. *Biophys. Chem.* **220**, 34–41 (2017).
47. S. Almeida *et al.*, Production of poly(Ga) in *C9orf72* patient motor neurons derived from induced pluripotent stem cells. *Acta Neuropathol.* **138**, 1099–1101 (2019).
48. B. D. Freibaum, J. P. Taylor, The role of dipeptide repeats in *C9orf72*-related Als-Ftd. *Front. Mol. Neurosci.* **10**, 35 (2017).
49. J. G. O'Rourke *et al.*, *C9orf72* bac transgenic mice display typical pathologic features of Als/Ftd. *Neuron* **88**, 892–901 (2015).
50. O. M. Peters *et al.*, Human *C9orf72* hexanucleotide expansion reproduces RNA foci and dipeptide repeat proteins but not neurodegeneration in Bac transgenic mice. *Neuron* **88**, 902–909 (2015).
51. D. A. Mordes *et al.*, Absence of survival and motor deficits in 500 repeat *C9orf72* bac mice. *Neuron* **108**, 775–783 (2020).
52. L. Nguyen *et al.*, Survival and motor phenotypes in Fvb C9–500 Als/Ftd Bac transgenic mice reproduced by multiple labs. *Neuron* **108**, 784–796 (2020).
53. J. M. Ward, *Pathology of Genetically Engineered Mice* (Iowa State University Press, ed. 1, Ames, p. 394 p, pp xi 2000).
54. W. A. Banks *et al.*, Passage of amyloid beta protein antibody across the blood-brain barrier in a mouse model of Alzheimer's disease. *Peptides* **23**, 2223–2226 (2002).
55. M. Bravo-Hernandez *et al.*, Spinal subpial delivery of Aav9 enables widespread gene silencing and blocks motoneuron degeneration in Als. *Nat. Med.* **26**, 118–130 (2020).